Biosensors and Bioelectronics 126 (2019) 485–492

Contents lists available at ScienceDirect

Biosensors and Bioelectronics

journal homepage: www.elsevier.com/locate/bios

The terahertz electromagnetically induced transparency-like metamaterials for sensitive biosensors in the detection of cancer cells

Xin Yan[a,b], Maosheng Yang[a], Zhang Zhang[b,*], Lanju Liang[a,b,**], Dequan Wei[a], Meng Wang[a], Mengjin Zhang[c], Tao Wang[c], Longhai Liu[d], Jianhua Xie[d], Jianquan Yao[b]

[a] School of Opto-Electronic Engineering, Zaozhuang University, Zaozhuang 277160, China
[b] Key laboratory of Opto-electronic Information Technology (Tianjin University), Ministry of Education, College of Precision Instrument and Opto-electronics Engineering, and Tianjin Key Laboratory of Low Dimensional Materials Physics and Preparing Technology, School of Science, Tianjin University, Tianjin 300072, China
[c] Department of Medical Oncology, Zaozhuang Municipal Hospital, Zaozhuang 277102, China
[d] Advantest (China) Co., Ltd, Shanghai 201203, China

ARTICLE INFO

Keywords:
Metamaterials
Electromagnetically induced transparency like (EIT-like) Fano resonance
Biosensors
Terahertz

ABSTRACT

A kind of novel biosensor based on the electromagnetic induced transparency like (EIT-like) metamaterials (MMs) have been proposed. It demonstrates that the symmetry-breaking double-splits ring resonators can realize the EIT-like plasmonic resonance, the according transparency window occurs at 1.67 THz. The coupled oscillators model illustrates that with the increase of asymmetry degree of double splits, the coupling between bright and dark mode is enhanced. Consequently, the non-radiative damping γ_2 grows from 1.45 to 1.85 THz and coupling coefficient κ from 3.46 to 4.49 THz^2, while the radiative damping γ_1 decreases from 11.5 to 9 THz. Such EIT-like MMs were evaluated in simulation as the refractive index sensors, which the theoretical sensitivity was calculated to 455.7 GHz/RIU (RIU, Refractive Index Unit) under 11 μm-thick analyte layer. Meanwhile, the dependence of full width at half maximum (FWHM) on analyte thickness was also studied. In experiments, it is found that the frequency shift Δf increases from 50 to 90 GHz when the oral cancer cells (HSC3) concentration improves from 1×10^5 to 7×10^5 cells/ml. The maximum experimental sensitivity approaches 900 kHz/cell ml^{-1} at 7×10^5 cells/ml. Additionally, the apoptosis of cancer cells under the effect of anti-cancer drug was investigated. It shows that with the increase of anti-cancer drug concentration from 1 to 15 μM and the extension of drug action duration from 24 to 72 h, the Δf changes from 140 to 70 GHz and 140–40 GHz, respectively. Besides, the corresponding FWHM also increases from 237.9 to 305.4 GHz and 237.8–337.6 GHz. The results measured by MMs biosensors and biological method exhibit a relatively good agreement, showing a great potential for cells measurement with the sensitive biosensors based on the EIT-like MMs.

1. Introduction

Electromagnetic metamaterials (MMs), composed by periodic-arranged subwavelength unit cells (meta-atoms), exhibit extraordinary properties that would not be possible with natural materials, having attracted great research interest in past decade (Smith et al., 2000; Shelby et al., 2001; Pendry, 2000; Fang et al., 2005; Schurig et al., 2006). The flexible modulation of MMs enables it to control the electromagnetic waves in a large degree of freedom. Such advantage make the MMs become a promising tool to engineer the waves as a desired manner, which brings in the widespread applications including hologram imaging (Zheng et al., 2015), communications (Zhang et al., 2015) and biological sensors (Wu et al., 2013; Danilov et al., 2018) due to the excellent capabilities such as beam steering (Yu et al., 2011), polarization conversion (Zhao et al., 2012) and strong localized fields (Kabashin et al., 2009). Notably, the unique response to electromagnetic waves of MMs is only determined by the geometry of structural configuration, so that the resonant features arisen from different order modes can be easily tailored under the careful optimization for resonant structure. Recently, a lot of attention have been paid to the electromagnetically induced transparency (EIT) phenomenon in MMs, which in fact is a quantum interference effect that decrease the absorption of incident waves over a narrow spectral region in a coherently driven atomic system (Zhang et al., 2008; Liu et al., 2017; He et al., 2017). In the following years, the EIT-like Fano resonance was also demonstrated in asymmetric configurations (Liu et al., 2009; Wang

* Correspondence to: College of Precision Instrument and Opto-electronics Engineering, Tianjin University, Tianjin 300072, China.
** Corresponding author at: School of Opto-Electronic Engineering, Zaozhuang University, Zaozhuang 277160, China.
E-mail addresses: twozhang@tju.edu.cn (Z. Zhang), lianglanju123@163.com (L. Liang).

https://doi.org/10.1016/j.bios.2018.11.014
Received 3 November 2018; Accepted 11 November 2018
Available online 14 November 2018

et al., 2018). In such type of plasmonic resonance, the small detuning between two excitation pathways make bright mode almost be suppressed, thus lead to the emergence of transparency window. Owing to the strong interference between two or more resonant modes, the EIT-like Fano resonant structures possess naturally sensitive property for the change of local environment. The underlying reasons are summarized as follows: a) a small perturbation can induce an obvious spectral variation including peak frequency shift and linewidth change thanks to the asymmetric lineshape; b) the suppression of radiative losses make the EIT-like Fano resonance only depend on the non-radiative damping, i.e., the intrinsic Drude loss of metal materials. That means any change that results in the lineshape variation can only be attributed to the change of external dielectric environment. Therefore, such sensitive property make MMs particularly more attractive for serving as biomedical and chemical sensing platforms compared with traditional biological detection as a result of unique advantages including non-labelling, non-destructive, time-conserving and low cost.

However, up to now, the real application of EIT-like MMs for biosensing have not been given a comprehensive insight. On one hand, some of works on MMs-based biosensors were reported (Park et al., 2014; Geng et al., 2017; Zhang et al., 2016), in which a frequency shift was presented under the effect of analytes due to the strong localized field. But the small theoretical sensitivity and the single criterion for judging the performance of biosensors make it hard to be applied in practical situations. On the other hand, most of existing MMs-based biosensors were designed to operate in the range of microwave bands and even in lower electromagnetic frequencies (1–10 MHz) (Stobiecka et al., 2017), yet the small variation of lineshape in a narrow bandwidth and the difficulty in miniaturized dimensions fabrication block these biosensors from developing toward an ultrasensitive stage and a wide application in the reality (He et al., 2010, 2011). In contrast, the terahertz (THz) waves gradually draws a lot of attention over the past few years. The great advancements acquired in radiative sources and time domain spectroscopy promote the rapid development of THz technology. The inherent characteristics of THz waves such as broadband, non-destructive, and transparency for most dielectrics make it be a promising candidate for the applications in communication and security (Nagatsuma et al., 2016; Federici and Moeller, 2010; Tonouchi, 2007). Especially, the low energy and fingerprint for molecules of THz waves also give rise to a suitable platform for biomedical detection and imaging. Nevertheless, owing to the limitations of sample size and thickness, the trace amount analysis for the in-situ diagnosis and examination is yet hard to be performed by THz spectral methods. Therefore, it is reasonable to consider that a novel biosensor which takes full advantages of THz waves and MMs should be proposed to satisfy the requirement of future biological sensing and disease diagnosis. In recent study of cell biology, a typical fluorescence detection, Flow Cytometry (FC) in visible band, is one of the most widely used methods in the detection of cells. In general, the fluorescences arise from different labels. Fluorescent chemicals may be used to label cell components. Unlike the proposed MMs biosensors, the cost of FC detection is not cheap and the detection preparation is complicated due to the irrecoverable consumption of fluorescence-labeled antibody and steps involved. Another method used in biological measurement is electrochemical measurements. Such technique can measure the potential difference between two electrodes. With electrochemical recordings, one of the electrodes will give a constant contribution to the total potential. Thus, a change in the total potential can be ascribed to a potential change at the measuring electrode. However, if the cells locate in the approximation of the electrodes, the activity of all the other cells will give noise, which may disturb the measurements. Also, the form of the recorded signals depends on the geometric position of the active cell with respect to the electrode, which complicates the problem.

Here, we have designed a symmetry-breaking double-splits ring resonator to realize the EIT-like plasmonic resonance. The coexistence of radiative mode (electric-dipole resonance) and non-radiative mode (magnetic-dipole resonance) gives rise to an interference between the two modes. Owing to the suppression of radiative damping, the transparency window emerges at 1.67 THz. The experimental measurement agrees well with the simulation results. Additionally, the effect of asymmetric degree s on the EIT-like resonance was also discussed. The coupled oscillators model was used to illustrate the mechanism of EIT-like phenomenon. With the increase of asymmetry degree of double splits, the coupling between two modes was enhanced, leading to the increase of non-radiative damping γ_2 from 1.45 to 1.85 THz and coupling coefficient κ from 3.46 to 4.49 THz^2, while the decrease of radiative damping γ_1 from 11.5 to 9 THz. Subsequently, the EIT-like MMs were evaluated in simulation as the refractive index sensors, the theoretical sensitivity under 11 μm-thick analyte layer was calculated to 455.7 GHz/RIU (RIU, Refractive Index Unit). In experiments, the oral cancer cells HSC3 were seeded on the MMs-based biosensors and the samples were measured by THz time domain spectroscopy (THz-TDS). It is found from results that the frequency shift distance Δf increases from 50 to 90 GHz when the cells concentration grows from 1×10^5 to 7×10^5 cells/ml, respectively. The maximum experimental sensitivity can approach 900 kHz/cell ml^{-1} at 7×10^5 cells/ml, which means that a cell per milliliter would lead to the shift of 900 kHz in frequency. Furthermore, the cells apoptosis was also monitored relied on the variation of Δf. The results demonstrate that with the increase of anticancer drug concentration from 1 to 15 μM and the extension of drug action duration from 24 to 72 h, the Δf changes from 140 to 70 GHz and 140–40 GHz, respectively. In addition, the full width at half maximum (FWHM) increases from 237.9 to 305.4 GHz and 237.8–337.6 GHz, respectively. The trend of Δf measured by THz-TDS acquired a relatively good agreement with the CCK-8 kits method that was measured by biological technique. Such novel EIT-like MMs biosensors exhibit significantly promising in future biomedical and biological detection.

2. Simulation and experimental method

The structural configuration of metal double splits ring resonators (DSRRs) supported on 25 μm-thick polyimide (PI) dielectric layer are shown in Fig. 1. The two splits are located asymmetrically for introducing the symmetric breaking. The whole MMs-based biosensor was schematically shown in Fig. 1(a). The incident THz waves penetrate the MMs from dielectric to metal layer, on which a number of cells have

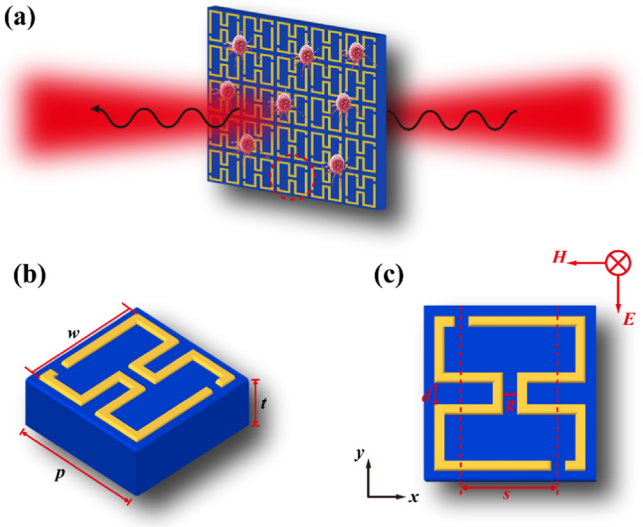

Fig. 1. (a) The geometric configuration of MMs-based biosensor, the THz waves normally incident through MMs, on which the biological analytes were adhered. (b) and (c) The structural configuration and the top view of unit cell consisting of MMs, respectively, the corresponding structural parameters are: $p = 50$ μm, $w = 44$ μm, $t = 25$ μm, $d = 6$ μm, $g = 4$ μm, $s = 28$ μm.

adhered. Fig. 1(b) and (c) give the specific configuration parameters, the detailed value can be found in figure caption. It is notably mentioned that the structural parameter *s* defined by the displacement of two splits along *x*-axis determines the asymmetric degree of DSRRs.

In our study, the spectral response of the designed DSRRs were numerically investigated by the full-wave numerical simulations, which are performed by commercial finite integration package CST Microwave Studio. The permittivity ε and tanδ of PI layer were 3.1 and 0.05, respectively. The magnetic and electric boundary conditions along *x* and *y* directions was adopted to model the *y*-polarized incident THz waves. Further, the real MMs samples were also fabricated for experimental measurements. The PI layer was firstly spin coated on silicon substrate. Then, the patterned of DSRRs were acquired by standard photolithography (ABM Mask Aligner) followed by the deposition process of 20 nm Ti and 200 nm Au layers, respectively (Denton Vacuum). Finally, the whole samples were immersed into the HF solution for few seconds, the PI layer with metal DSRRs supported upon would be peeled off from silicon substrate. Subsequently, the resonant features of flexible MMs samples were measured in THz-TDS system (ADVANTEST TAS7500SU). To demonstrate the potentials of EIT-like MMs in serving as biosensors, the oral-cancer cells HSC3 were seeded and cultured on the surface of DSRRs. Such cells-culturing process absolutely follows the culturing method of adherent cells. The adhered cells were grown at 37°, 10% concentration for CO_2 (Thermo Fisher Scientific) in culturing solution, which is mainly consist of Dulbecco's Modified Eagle's medium (DMEM, Gibco) supplemented with 10% fetal bovine serum (FBS, Gibco) and 1% combination of penicillin and streptomycin (Gibco). In this case, the cells would form as single layer due to the contact inhibition. After the cellular morphology reached normal state, the trypsin-EDTA (Gibco) would be added to digest cells from the walls of culturing bottles followed by the preparation of cells suspension by introduced a certain number of culturing solution. After the cells suspension were seeded on the surface of MMs, the samples were finally cultured again at the environment mentioned before. The sample manufacturing and cells seeding process was schematically shown in Fig. 2. Cancer cells apoptosis was monitored by a Cell Counting Kit-8 (CCK-8, Dojindo). Briefly, 100 µl of HSC3 cell suspension (2000 cells/ml) were plated in 24-well plates and pre-incubated for 12 h. Subsequently, different concentrations of anti-cancer drug were added in and incubated for 24 h. Then, 10 µl of CCK-8 solution was added to each well and the number of cells was counted at the indicated time points by measuring the absorbance at 450 nm using Epoch Microplate Spectrophotometer.

3. Results and discussion

In order to understand the underlying resonant mechanism of designed DSRRs structures, the transmission of MMs was simulated and measured, respectively, seen from Fig. 3(a). It is shown that the experimental and simulation results agree well except for slight difference in intensity at two dips which located at 1.15 and 1.87 THz. The reason may be contributed to the difference of adopted simulation conditions from the actual cases and the fabrication error in the experimental process. It is also interesting to find that a transmission peak with 55% efficiency appears at around 1.67 THz, while the absorption dip at this frequency reduces to 30%, as black and blue line shown, respectively, in Fig. 3(a). Owing to the observation of this weak transparency phenomenon, it reasonably to believe that there may be some mode coupling effect in our designed DSRRs structures. To further investigate the physical mechanism, the electric field, magnetic field in *z* axis and the surface charge density at three different frequencies were monitored and shown in Fig. 3(b)–(g), respectively. For 1.20 THz, signed as region I, the transmission almost falls to zero. The corresponding electric field shown in Fig. 3(b) implies that an electric dipole resonant mode was generated at this frequency. Meanwhile, the incomplete semi-circulating currents is formed on the two sides of the metal trace, enclosed by black dash circle. It is because of such quasi-circulating surface currents that induces the weak magnetic field which only located on two sides of metal rings, as seen in Fig. 3(c). When the frequency increases to 1.67 THz, as region II, it is obviously observed that a pair of electric quadrupole are formed, seen in Fig. 3(d). At the same time, two parts of complete circulating currents is flowing along the upper and bottom rings, enclosed by black dash circles in Fig. 3(e), respectively. Thanks to such circulating currents along the electric quadrupole, the out-phase magnetic fields are induced inside the space surrounded by metal rings and the strength is enhanced, which results in the generation of magnetic dipoles resonance. Such similar case was also observed in other research work (Wang et al., 2013). From the above analysis, it is interestingly to found that the electric field distribution transforms into the quadrupole resonant mode, which is non-radiative damping. A possible explanation for this change of resonant mode might be that the magnetic dipole/electric quadrupole resonance (dark mode) couples with the electric dipole (bright mode) originated from 1.20 THz, the destructive interference leads to the suppression of bright mode and couples the energy to the dark mode, thus the quadrupole resonance is dominant under such condition. Because of the electric dipole suppression, the radiative losses are dramatically reduced and the transmission improves accordingly. This can be verified by the black line in Fig. 3(a), in which the transmission increases to 55% at the frequency of 1.67 THz while the absorption decreases to 30%. At the third region III that locates at 2.0 THz, it shows that the electric quadrupole transforms to dipoles mode again, and the out-phase magnetic fields did not locate inside the metal rings due to the incomplete circulating currents, as shown in black dash circles of Fig. 3(g). Such change implies that the interference reduced again with the increase of frequency. In this case, the radiative losses are dominant and the transmission window disappears.

Based on above analysis, it is shown that different resonant types own different electric field distribution at the splits position. For example, at 1.20 THz, the electric field is distributed in-phase on both ends of splits, while it becomes out-phase when the frequency improves to 1.67 THz. Therefore, the splits position is considered to be related with the property of EIT-like resonance. To further investigate the effect of the asymmetric degree of splits on the behavior of EIT-like MMs, the structures with different parameter *s* are designed and the model of coupled harmonic oscillators is used to explain the mechanism of two mode coupling. This model treats the bright and dark modes as two harmonic oscillators, the interference can be analytically described by the Lorentz model as (Gu et al., 2012; Xiao et al., 2018):

$$\begin{aligned} &\ddot{x}_1 + \gamma_1\dot{x}_1 + \omega_0^2 x_1 + \kappa x_2 = E, \\ &\ddot{x}_2 + \gamma_2\dot{x}_2 + (\omega_0 + \delta)^2 x_2 + \kappa x_1 = 0 \end{aligned} \tag{1}$$

where x_1, x_2, γ_1 and γ_2 are the resonant amplitudes and the losses of bright and dark modes, respectively. δ denotes the detuning of the resonant frequency of dark mode oscillator from the bright mode one. κ is the coupling coefficient between the two oscillators. By solving the Eq. (1) with the approximation ω-$\omega_0 \ll \omega_0$, the susceptibility χ is obtained:

$$\chi = \chi_r + i\chi_i \propto \frac{(\omega - \omega_0 - \delta) + i\frac{\gamma_2}{2}}{\left(\omega - \omega_0 + i\frac{\gamma_1}{2}\right)\left(\omega - \omega_0 - \delta + i\frac{\gamma_2}{2}\right) - \frac{\kappa^2}{4}} \tag{2}$$

As well-known, the imaginary part of susceptibility χ_i is proportional to the energy losses, therefore the transmission *T* can be acquired through $T = 1\text{-}g\chi_i$, in which *g* represents the geometric parameter, indicating the coupling strength of the bright mode with the incident electric field *E*. By using Eq. (2), the transmission *T* of structures with different asymmetric degree *s* were analytically fitted according to the model of coupled harmonic oscillators, as shown in Fig. 4. It can be found from Fig. 4(a)–(d) that the theoretically fitting results exhibit a relatively good agreement with the simulation. The transmission and resonant frequency under different *s* are extracted, respectively, as

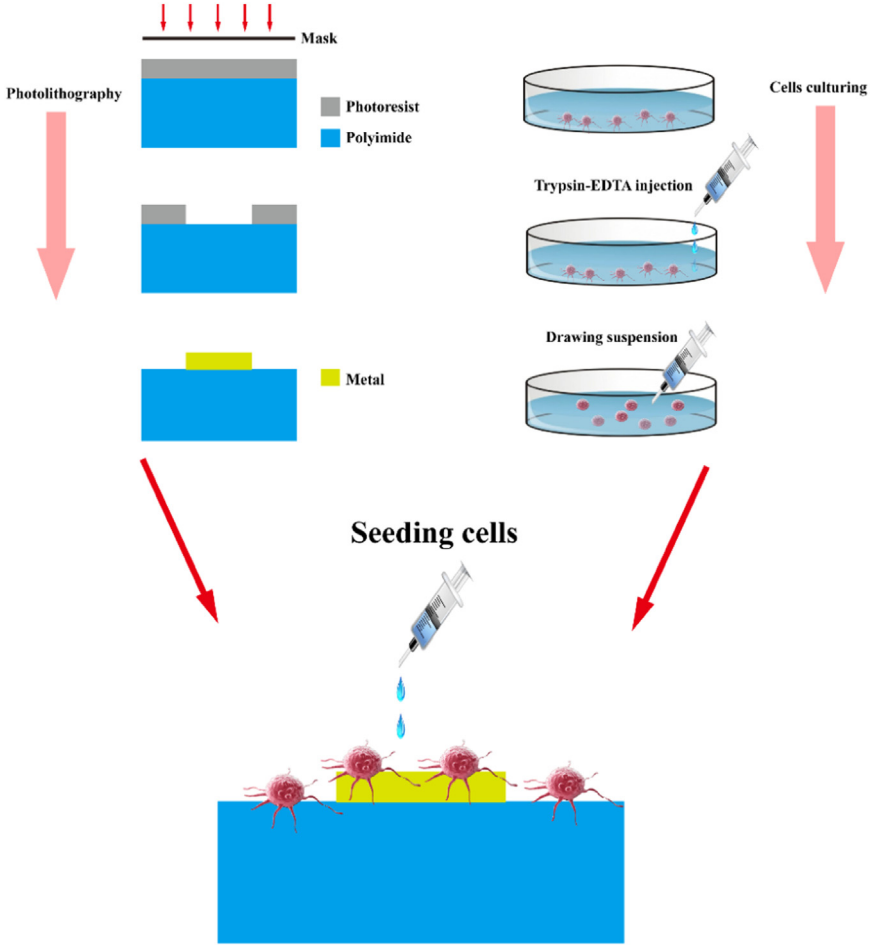

Fig. 2. The schematic of seeding cells method on MMs-based biosensors including traditional photolithography manufacturing steps and cells culturing process.

shown in Fig. 4(e). It is suggested that with the increase of asymmetric degree *s,* in addition to slightly blue-shift in frequency from 1.59 to 1.61 THz, the transmission efficiency of peak frequency raised linearly from 0.49 to 0.55. Such trend demonstrates that the enhancement of symmetric-breaking brings significant interference, which leads to the radiative losses being suppressed further, thus the transmission window manifest higher efficiency with the increase of *s*. Additionally, the dependence of fitted parameters according to Eq. (2) on the asymmetric degree are shown in Fig. 4(f). It can be seen that the radiative damping item represented by γ_1 is reduced from 11.5 to 9 THz with the asymmetric degree increasing while the non-radiative damping item γ_2 added from 1.45 to 1.85 THz. This also accords with our earlier observation, which shows that the stronger coupling effect induced between bright and dark modes gives rise to the suppression of radiative losses. More explicitly, shown in Fig. 4(f), the enhancement of coupling coefficient κ from 3.46 to 4.49 THz^2 with the growing asymmetric degree verified this conclusion. The stronger coupling between two modes would lead to more prominent suppression of radiative losses. Therefore, when the asymmetric degree *s* approaches the largest value, the radiative losses would totally be suppressed. For this reason, the EIT-like Fano resonance of DSRRs only depends on the non-radiative damping, i.e., the intrinsic Drude loss of metal materials. This characteristic is great of benefited to the sensing because any change that results in the lineshape variation can only be attributed to the change of external dielectric environment. Thus, the ultrasensitive property has significant possibility to be realized in such structural configurations.

Further opportunities were made available with the attempts to exploit the EIT-like property of MMs in the biological and biochemical field. Firstly, the refractive index sensors based on MMs were theoretically calculated. An analyte layer was selected to add onto the DSRRs structures. By changing the refractive index of analyte under the thickness of 11 μm, the theoretical sensitivity defined by the derivative of transparency frequency shift to the change of refractive index can be acquired. It can be found from Fig. 5(a) that with the refractive index varies from 1 to 1.6, the transparency peak redshift from 1.71 to 1.38 THz. The according relative frequency shift Δf, defined as the absolute value of peak frequency distance between curve of MMs with and without analyte layer, were extracted and displayed in Fig. 5(d). The linear relationship of Δf-n function is observed in the graph, and the sensitivity S can be obtained by calculating the corresponding derivative of Δf-n curve. The theoretical sensitivity of refractive index sensor based on our designed EIT-like MMs approaches 455.71 GHz/RIU (RIU, Refractive Index Unit). This result is higher than that of our other reported work (Zhang et al., 2018). Furthermore, the thickness of analyte layer can also affect the frequency shift of MMs. From Fig. 5(b), it can be seen that when the thickness grows from 1 to 11 μm under the fixed refractive index of 1.6, the frequency shift Δf is improved from 112 to 267 GHz. In addition, it also shows that the effect of analyte layer thickness on the Δf appears a nonlinear trend. In other words, there must be a limit value for Δf. Once exceeds this value, the Δf would not increase significantly anymore no matter how large the thickness is. As seen in Fig. 5(e), when the thickness reached 11 μm, the slope of Δf-thickness curve turns to be small. It is implied that after this thickness, the sensitivity almost keep unchanged despite the increase of analyte thickness. On the other hand, the full width at half maximum (FWHM) of transmission changes with the analyte thickness as well. As shown in Fig. 5(d), the FWHM reduces from 394.6 to 204.3 GHz when the analyte thickness improves from 1 to 11 μm. Besides, the parameter Occupying

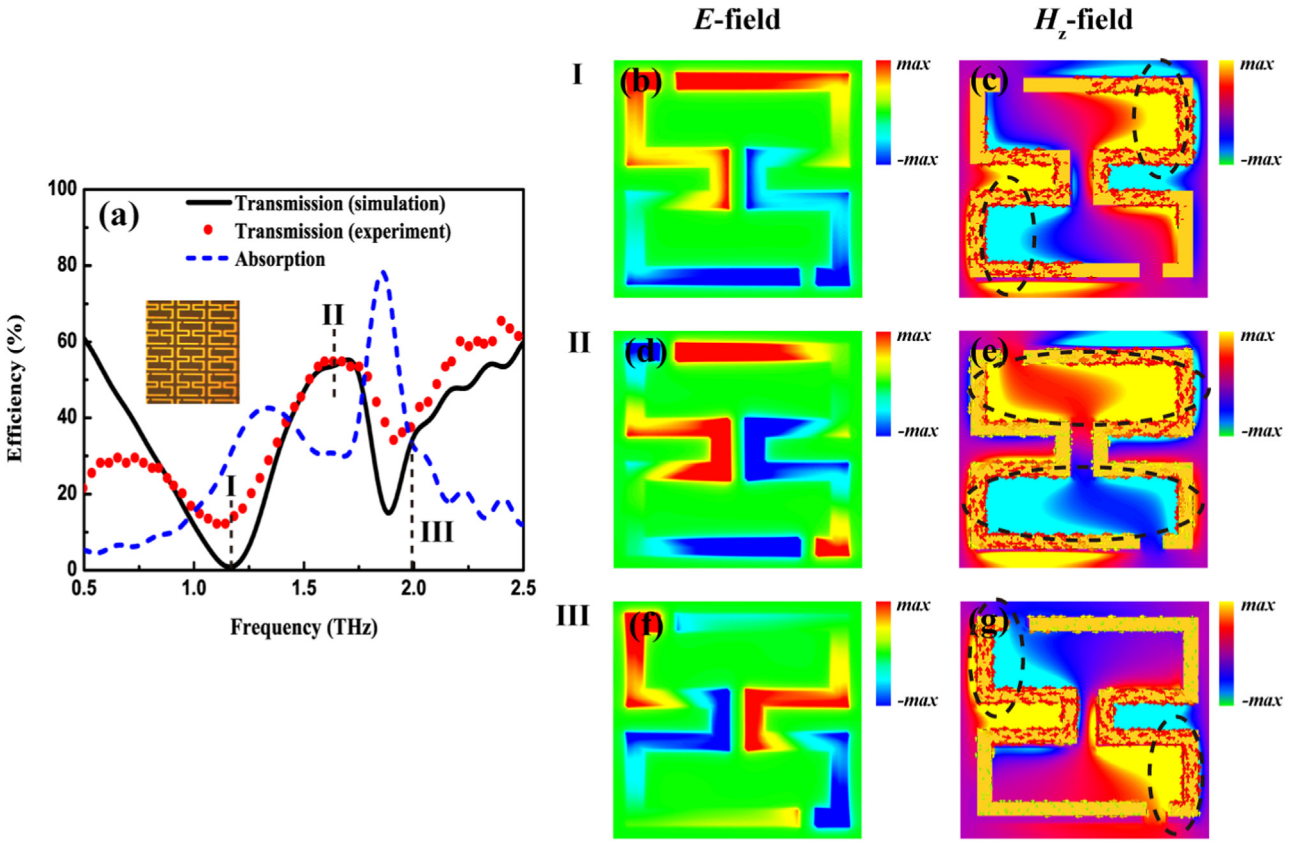

Fig. 3. (a) The transmission curves obtained by simulation (black line) and experiment (red dots line), respectively. The absorption (blue dash line) was also given in here. The inset has shown the microphotograph of designed MMs. (b)–(g) The corresponding electric, magnetic field and surface current at three frequency regions marked by I, II and III in (a), respectively (For interpretation of the references to color in this figure legend, the reader is referred to the web version of this article.).

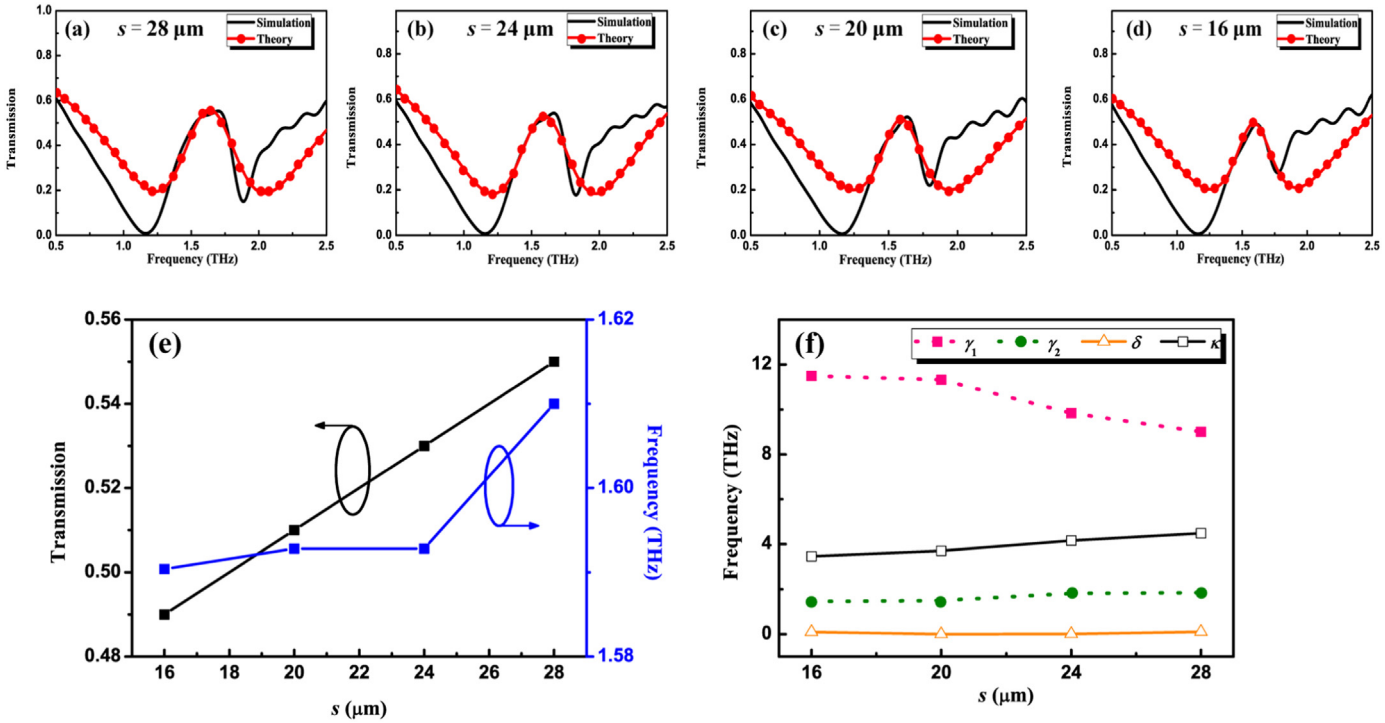

Fig. 4. (a)–(d) The transmission curves obtained by simulation (black line) and theoretical calculations (red circles line) for s = 28, 24, 20 and 16 μm, respectively. (e) The dependence of transmission (black line) and resonant frequency (blue line) on the asymmetric degree s, respectively. (f) The dependence of γ_1, γ_2, δ and κ extracted by fitting the transmission curves according to Eq. (2) on the asymmetric degree s, respectively. The unit of κ is THz^2 (For interpretation of the references to color in this figure legend, the reader is referred to the web version of this article.).

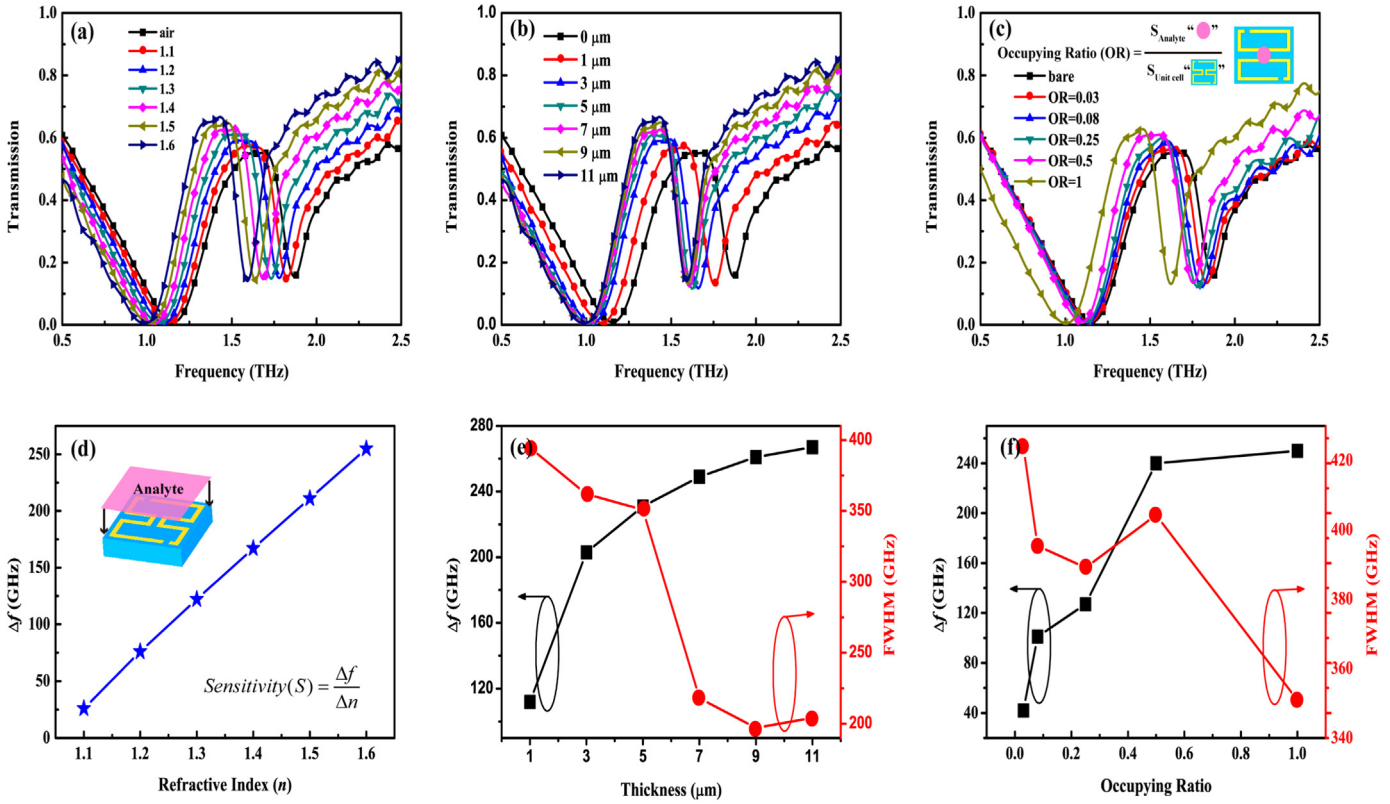

Fig. 5. (a) The dependence of transmission on the analyte refractive index increasing from 1 to 1.6 under the thickness of 11 μm. (b) The dependence of transmission on the analyte thickness increasing from 0 to 11 μm under the fixed refractive index of 1.6. (c) The dependence of transmission on the occupying ratio (OR) increasing from 0.03 to 1 under the fixed refractive index of 1.6 and the thickness of 6 μm. (d) The frequency shift under the different refractive index of analyte extracted from (a). (e) The frequency shift and FWHM under different analyte thickness extracted from (b). (f) The frequency shift and FWHM under different OR extracted from (c).

Ratio (OR) is defined to illustrate the influence of the analyte numbers on resonant feature of MMs. From Fig. 5(c), a red-shift in resonant peak from 1.69 to 1.45 THz with the increase of OR value have been displayed. In order to give a clear exhibition, the dependence of Δf and FWHM on the OR value are extracted and shown in Fig. 5(f), respectively. The results suggest that with the increase of OR, the Δf improves from 42 to 250 GHz while the FWHM reduces from 422 to 350 GHz. Based on the physical mechanism of EIT-like resonant feature, the change in FWHM can be attributed to the fact that the analyte layer can absorb part of incident THz waves, thus effectively reducing the radiative losses of metal DSRRs structures, and narrow the transmission linewidth. Such variation can be served as another new index for evaluating the performance of EIT-like MMs biosensors.

As a result of desirable theoretical sensitivity and linewidth change, it is great promising to apply such MMs as a biosensor platform with advantages of high sensitive, non-labelling and low cost. To investigate the sensitive performance of EIT-like MMs for biosensors, the oral cancer cells HSC3 was selected as our analytes to culture onto the surface of MMs. As well known, the successful detection of cancer cells in a trace amount scale plays an important role to the initiate diagnosis and therapies for cancer. Therefore, the ability to detect the variation of cell concentration by measuring the corresponding THz spectra of MMs biosensors is of great concerns in our experiments. As shown in Fig. 6(a), it is found that the transmission is decreased when the cells concentration is higher (7×10^5 cells/ml). But in Fig. 7(a) and (d), the lower transmission is observed in lower cells concentration (more cells were killed under the effect of anti-cancer drug). Such two phenomena are contradictory. Therefore, we believe that the appearance of such unusual response is not related with some certain physical phenomenon, but the individual fabrication difference of samples. Apart from the samples fabrication error, the circumstances of measurement at that moment can also affect the transmission as a result of the sensitivity to humidity of THz waves. Therefore, it is normal to find that the transmission of each sample is different. For this reason, most of research works did not evaluate the property of biosensors by analyzing the transmission intensity, but the resonant frequency shift. After the measurement of resonant frequency, it is suggested that for different cells concentrations, the resonant peak of designed structure red shift from the frequency of 1.65 THz, which originated from the bare MMs sample. To demonstrate this change more explicitly, the frequency shift Δf under different cells concentrations was shown in Fig. 6(b) as well. The micrograph of bare sample and the sample with certain cells concentration cultured on are also shown in the insets, the color-enhanced images are given to make a convenient comparison. With the cell concentration increasing from 1×10^5 to 7×10^5 cells/ml, the Δf grows from 50 to 90 GHz. This result implies that the resonant peak of EIT-like MMs is sensitive to the variation of cells concentration. Moreover, the slope of Δf tend to be gently with the augment of cells concentration, which suggests a finite sensitivity in the real situations. In our experiment, by calculating the sensitivity defined as $S = \Delta f / \Delta c$, where Δc represents the variation of cells concentration, the maximum sensitivity approaches 900 kHz/cell ml^{-1} at 7×10^5 cells/ml, which means that a cell per milliliter would lead to the shift of 900 kHz in peak frequency. This property can help us build the relationship of cells concentration with the resonant peak shift, and supply an alternative way to investigate the cancer cells activity from physical perspective.

Among various cell activities, apoptosis is one of the most significant characteristics for evaluating the evolution of cancer cells. The anti-cancer drugs have been demonstrated effective for killing cancer cells and promoting cancer cells apoptosis. In order to prove the promising application of our designed biosensors based on the EIT-like MMs in the detection of cancer cells apoptosis, the transmission of

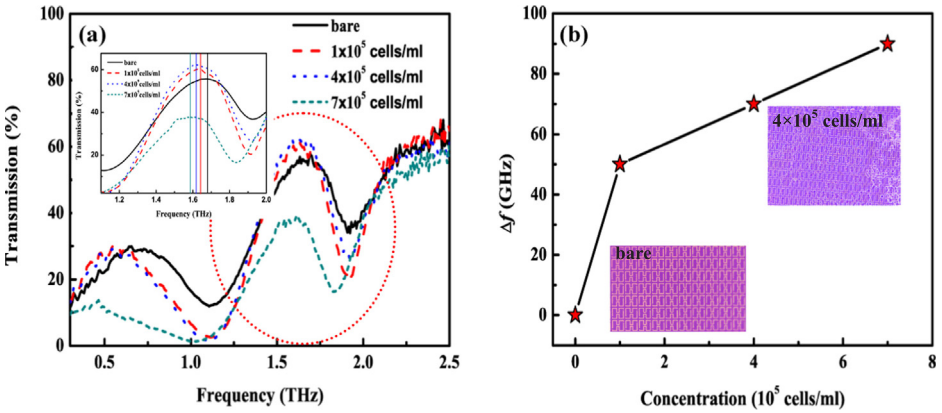

Fig. 6. (a) The transmission of EIT-like MMs under different cancer cells concentrations from 1 to 7×10^5 cells/ml, respectively. The inset shows the exlarge version of resonant peak, the according position were marked by vertical lines. (b) The dependence of resonant peak shift Δf on different cells concentrations extracted from (a), the insets show the micrograph of bare sample and the sample with cells concentration of 4×10^5 cells /ml cultured on.

biosensors under different concentrations of cisplatin, a kind of anti-cancer drug, and different drug action time were measured, respectively. Before exerting cisplatin, the original cells concentration of 2×10^6 cells/ml were cultured on the surface of MMs biosensors. The samples were divided into two groups and treated by different conditions. The indicated cisplatin concentrations from 1 to 15 μM under fixed action time of 24 h and indicated drug action time from 24 to 72 h under fixed cisplatin concentration of 1 μM were performed in our experiments, respectively. The measurement results are shown in Fig. 7. It can be seen from Fig. 7(a) that when the cisplatin concentration is raised, the resonant peak occurs a relative blue-shift, the corresponding Δf were shown in Fig. 7(b), which shows the Δf decreasing from 140 to 70 GHz. Based on the rule of peak frequency shift mentioned before, it suggests that the cells concentration is reduced due to the cell-killing effect of anti-cancer drug. In other words, the larger cisplatin concentration would promote the cell apoptosis more prominently. Such conclusion can be verified by the tests of the biological CCK-8 kits method. Also, the biological measurement shown as dashed line in Fig. 7(b) implies that with the concentration of cisplatin improving from 1 to 15 μM, the apoptosis is accordingly accelerated from 5.3% to 35.4%, thus giving rise to the data in graph which have been transformed as the complement of apoptosis (1-Apoptosis) in percentage. The two curves show a relatively good agreement. More directly, the FWHM of transmission under three conditions are also extracted, as seen in Fig. 7(c). The FWHM varying from 237.9 to 305.4 GHz also agrees well with the biological apoptosis. Interestingly, the similar transmission linewidth variation in the experimental and the simulation results reveals that the increasing cells numbers can effectively absorb

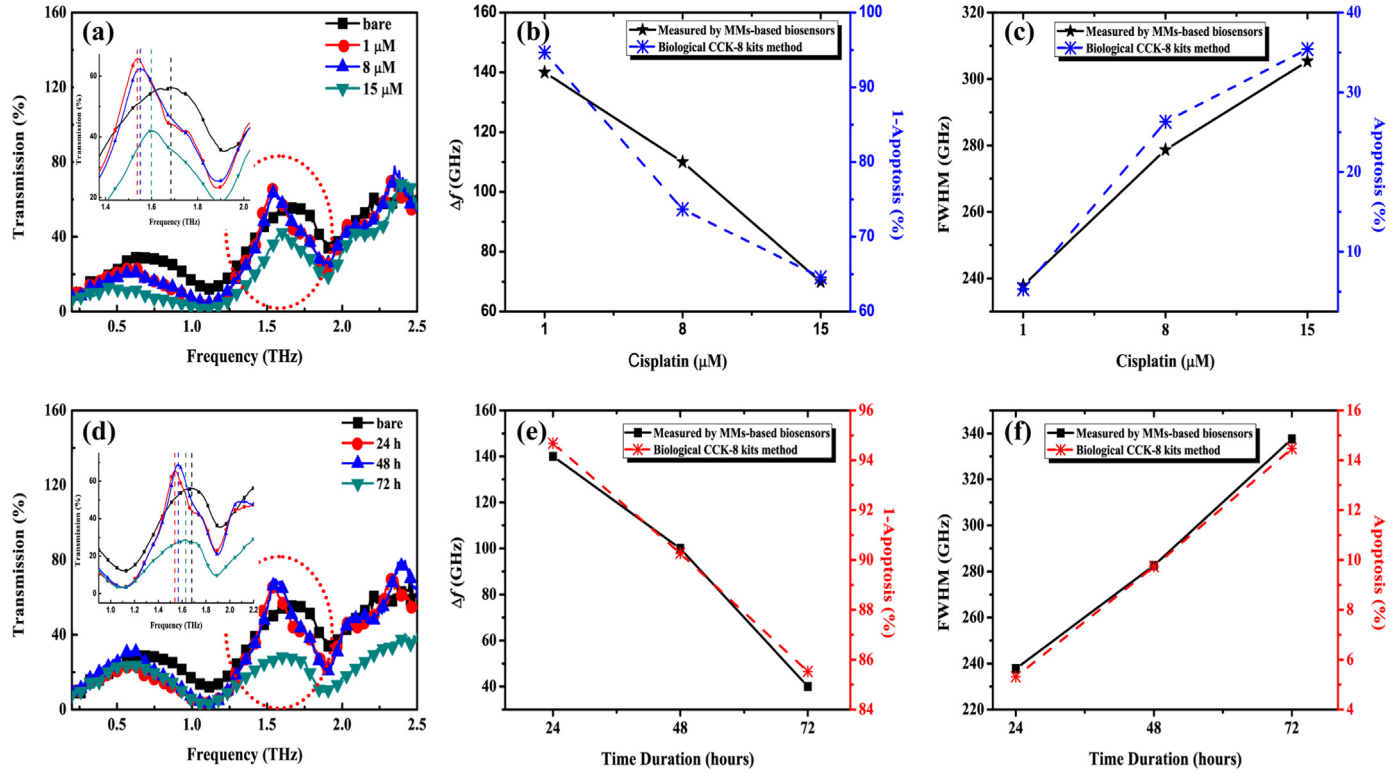

Fig. 7. (a) The transmission of EIT-like MMs biosensors under different cisplatin concentrations from 1 to 15 μM, the bare case was also given for comparison. (b) The dependence of resonant peak shift Δf extracted from (a) and the apoptosis measured by the biological CCK-8 kits method on different cisplatin concentrations. (c) The dependence of the FWHM of transmission line extracted from (a) and the apoptosis measured by the biological CCK-8 kits method on different cisplatin concentrations. (d) The transmission of EIT-like MMs biosensors under different drug action time from 24 to 72 h. (e) The dependence of resonant peak shift Δf extracted from (d) and the apoptosis measured by the biological CCK-8 kits method on different drug action time. (f) The dependence of the FWHM of transmission line extracted from (d) and the apoptosis measured by the biological CCK-8 kits method on different drug action time.

the THz waves, leading to the reduction of radiative losses generated by metal DSRRs structures. Furthermore, the agreement acquired between the dependence of Δf and FWHM on the cisplatin concentration measured by the MMs biosensors and the apoptosis obtained by the biological method implies the feasibility of biosensors based on sensitive EIT-like MMs to realize the cells measurement. Similarly, in addition to the effect of drug concentration, the apoptosis of cancer cells under different drug action time is investigated as well. From Fig. 7(d), it shows that with the extend of drug action time from 24 to 72 h, the resonant peak also exhibits blue-shift, which reveals the decrease of cancer cells concentration. The dependence of extracted frequency shift Δf and the biological CCK-8 kits measurements on the drug action time are shown in Fig. 7(e), respectively. A good agreement achieved between the curve of Δf which decreases from 140 G to 40 GHz and the curve of 1-Apoptosis from 94.7% to 85.5% demonstrates that with the prolong of drug action time, the cancer cells are killed effectively, the apoptosis of cancer cells is accelerated. In addition to the Δf, the FWHM displays an excellent agreement with the apoptosis measured by biological method, seen in Fig. 7(f). The FWHM of transmissions under three drug action time broaden from 237.8 G to 337.6 GHz, which is almost coincided with the apoptosis increasing from 5.3% to 14.5%. Therefore, based on the above analysis of cancer cells apoptosis, it is found that both the Δf and the FWHM detected by MMs biosensors agree well with the measurement of biological method, which demonstrates the significant underlying potentials of our designed MMs biosensors in the application of cancer cells detection, and supply a new way to realize the fast and low-cost biosensors from physical perspective.

4. Conclusions

In this paper, the MMs composed of DSRRs structures were designed in THz frequency range. The specific asymmetric double splits induce the EIT-like resonant peak at 1.67 THz. The corresponding electric, magnetic fields distribution and surface currents imply that the distinct electric dipole resonance (bright mode) and the weak magnetic dipole/electric quadrupole resonance (dark mode) occurs coupling, which leads to the destructive interference and the suppression of bright mode. For this reason, the dark mode, i.e., quadrupole resonance is dominant. Consequently, the transparency window is induced due to the dramatically reduced radiative losses at such frequency. The coupled oscillators model is used to illustrate the mechanism of EIT-like phenomenon. It is found that with the increase of asymmetry degree of double splits, the coupling between two modes is enhanced, giving rise to the increase of non-radiative damping γ_2 from 1.45 to 1.85 THz and coupling coefficient κ from 3.46 to 4.49 THz^2, while the radiative damping γ_1 decreasing from 11.5 to 9 THz. Under such condition, the EIT-like Fano resonance of DSRRs only depends on the non-radiative damping, i.e., the intrinsic Drude loss of metal materials. This characteristic is great of benefit to the sensing because any change that results in the lineshape variation can only be attributed to the change of external dielectric environment. Simulation results demonstrate that the maximum theoretical sensitivity can approach 455.71 GHz/RIU. Additionally, it shows that the frequency shift Δf tend to change slowly when the analyte thickness is beyond 11 μm. In experiments, the different cancer cells concentrations were cultured on the MMs biosensors. The Δf increases from 50 to 90 GHz when the cells concentration is improved from 1×10^5 to 7×10^5 cells/ml, respectively. The maximum experimental sensitivity approaches 900 kHz/cell ml^{-1} at 7×10^5 cells/ml, which means that a cell per milliliter would lead to the shift of 900 kHz in peak frequency. Based on the sensitivity of Δf to the cell concentration, the apoptosis of cancer cells under the effect of anti-cancer drug was investigated. The results reveal that with the increase of anti-cancer drug concentration from 1 to 15 μM and the extension of drug action time from 24 to 72 h, the Δf changes from 140 to 70 GHz and 140–40 GHz, respectively, while the FWHM increases from 237.9 to 305.4 GHz and 237.8–337.6 GHz, respectively. The results measured by the MMs biosensors and biological method present a relatively good agreement, suggesting the feasibility of biosensors based on sensitive EIT-like MMs to realize the cells measurement, and supplying a new way to realize the fast and low-cost cells detection from physical perspective.

Acknowledgements

This work was supported by the National Natural Science Foundation of China (Grant numbers 61701434, 61735010 and 61675147); the Open Fund of Key laboratory of Opto-electronic Information Technology, Ministry of Education (Tianjin University), Key Laboratory of Optoelectronic information functional materials and Micro-Nano devices in Zaozhuang, the China Postdoctoral Science Foundation (Grant number 2015M571263); the Natural Science Foundation of Shandong Province (Grant numbers ZR2017MF005, ZR2018LF001); the National key Research and Development Program of China (Grant numbers 2017YFA0700202, 2017YFB1401203); A Project of Shandong Province Higher Education Science and Technology Program (Grant number J17KA087); the Programe of Independent and Achievement Transformation plan for Zaozhuang (Grant numbers 2016GH19, 2016GH31); Zaozhuang Engineering Research Center of Terahertz.

References

Danilov, A., Tselikov, G., Wu, F., Kravets, V.G., Ozerov, I., Bedu, F., Grigorenko, A.N., Kabashin, A.V., 2018. Biosens. Bioelectron. 104, 102–112.
Fang, N., Lee, H., Sun, C., Zhang, X., 2005. Science 308, 534–537.
Federici, J., Moeller, L., 2010. J. Appl. Phys. 107, 111101.
Geng, Z., Zhang, X., Fan, Z., Lv, X., Chen, H., 2017. Sci. Rep. 7, 16378.
Gu, J., Singh, R., Liu, X., Zhang, X., Ma, Y., Zhang, S., Maier, S.A., Tian, Z., Azad, A.K., Chen, H.T., Taylor, A.J., Han, J., Zhang, W., 2012. Nat. Commun. 3, 1151.
He, X., Yang, X., Lu, G., Yang, W., Wu, F., Yu, Z., Jiang, J., 2017. Carbon 123, 668–675.
He, X.J., Wang, Y., Wang, J.M., Gui, T.L., 2010. Microsyst. Technol. 16, 1735–1739.
He, X.J., Qiu, L., Wang, Y., Geng, Z.X., Wang, J.M., Gui, T.L., 2011. J. Infrared Millim. Terahertz Waves 32, 902–913.
Kabashin, A.V., Evans, P., Pastkovsky, S., Hendren, W., Wurtz, G.A., Atkinson, R., Pollard, R., Podolskiy, V.A., Zayats, A.V., 2009. Nat. Mater. 8, 867–871.
Liu, M., Tian, Z., Zhang, X., Gu, J., Ouyang, C., Han, J., Zhang, W., 2017. Opt. Express 17, 19844–19855.
Liu, N., Langguth, L., Weiss, T., Kästel, J., Fleischhauer, M., Pfau, T., Giessen, H., 2009. Nat. Mater. 8, 758–762.
Nagatsuma, T., Ducournau, G., Renaud, C.C., 2016. Nat. Photonics 10, 371–379.
Pendry, J., 2000. Phys. Rev. Lett. 85, 3966–3969.
Park, S.J., Hong, J.T., Choi, S.J., Kim, H.S., Park, W.K., Han, S.T., Park, J.Y., Lee, S., Kim, D.S., Ahn, Y.H., 2014. Sci. Rep. 4, 4988.
Smith, D.R., Padilla, W.J., Vier, D.C., Nemat-Nasser, S.C., Schultz, S., 2000. Phys. Rev. Lett. 84, 4184–4187.
Shelby, R.A., Smith, D.R., Schultz, S., 2001. Science 292, 77–79.
Schurig, D., Mock, J.J., Justice, B.J., Cummer, S.A., Pendry, J.B., Starr, A.F., Smith, D.R., 2006. Science 314, 977–980.
Stobiecka, M., Jakiela, S., Chalupa, A., Bednarczyk, P., Dworakowska, B., 2017. Biosens. Bioelectron. 88, 114–121.
Tonouchi, M., 2007. Nat. Photonics 1, 97–105.
Wu, X., Quan, B., Pan, X., Xu, X., Lu, X., Gu, C., Wang, L., 2013. Biosens. Bioelectron. 42, 626–631.
Wang, Y., Leng, Y., Wang, L., Dong, L., Liu, S., Wang, J., Sun, Y., 2018. Appl. Phys. Express 11, 062001.
Wang, J., Fan, C., He, J., Ding, P., Liang, E., Xue, Q., 2013. Opt. Express 21, 2236–2244.
Xiao, S., Wang, T., Liu, T., Yan, X., Li, Z., Xu, C., 2018. Carbon 126, 271–278.
Yu, N., Genevet, P., Kats, M.A., Aieta, F., Tetienne, J.P., Capasso, F., Gaburro, Z., 2011. Science 334, 333–337.
Zheng, G., Mühlenbernd, H., Kenney, M., Li, G., Zentgraf, T., Zhang, S., 2015. Nat. Nanotechnol. 10, 308–312.
Zhang, Y., Qiao, S., Liang, S., Wu, Z., Yang, Z., Feng, Z., Sun, H., Zhou, Y., Sun, L., Chen, Z., Zou, X., Zhang, B., Hu, J., Li, S., Chen, Q., Li, L., Xu, G., Zhao, Y., Liu, S., 2015. Nano Lett. 15 (5), 3501–3506.
Zhao, Y., Belkin, M.A., Alù, A., 2012. Nat. Commun. 3, 870.
Zhang, S., Genov, D.A., Wang, Y., Liu, M., Zhang, X., 2008. Phys. Rev. Lett. 101, 047401.
Zhang, C., Liang, L., Ding, L., Jin, B., Hou, Y., Li, C., Jiang, L., Liu, W., Hu, W., Lu, Y., Kang, L., Xu, W., Chen, J., Wu, P., 2016. Appl. Phys. Lett. 108, 241105.
Zhang, Z., Ding, H., Yan, X., Liang, L., Wei, D., Wang, M., Yang, Q., Yao, J., 2018. Opt. Mater. Express 8, 659–667.